Supplemental material for

Ultrafast all-optical manipulation of the charge-density-wave in VTe$_2$

Manuel Tuniz,[1] Davide Soranzio,[2] Davide Bidoggia,[1] Denny Puntel,[1] Wibke Bronsch,[3]

Steven Johnson,[2] Maria Peressi,[1,4] Fulvio Parmigiani,[1,5,3] and Federico Cilento[3,*]

[1]*Dipartimento di Fisica, Università degli Studi di Trieste, Italy*

[2]*Institute for Quantum Electronics,*

Eidgenössische Technische Hochschule (ETH) Zürich, 8093 Zurich, Switzerland

[3]*Elettra - Sincrotrone Trieste S.C.p.A.,*

Strada Statale 14, km 163.5, Trieste, Italy

[4]*ICSC - Italian Research Center on High Performance Computing,*

Big Data and Quantum Computing

[5]*International Faculty, University of Cologne,*

Albertus-Magnus-Platz, 50923 Cologne, Germany

(Dated: November 23, 2023)

CONTENTS

* federico.cilento@elettra.eu

I. HIGH-TEMPERATURE CRYSTAL STRUCTURE OF VTe$_2$

The high-temperature crystal structure of VTe$_2$ consists in a trigonal unit cell with lattice parameters $a = 3.60$ Å and $c = 7.70$ Å. The same energy cutoffs and pseudopotentials employed for the simulations of the CDW phase were used also here while a different $11 \times 11 \times 9$ k-points mesh was employed in this case.
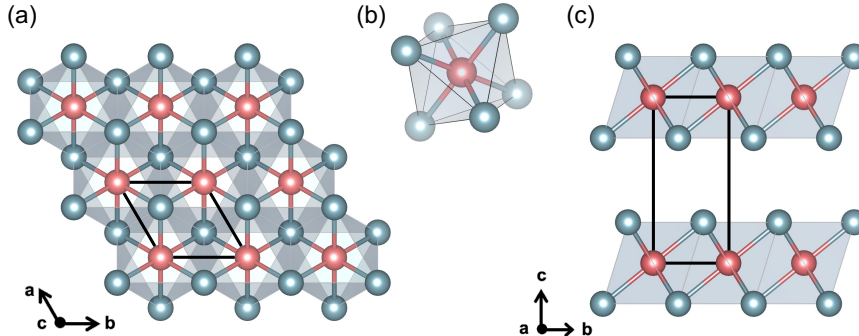

FIG. S1.   (a) Top view of the high-temperature crystal structure of VTe$_2$. (b) Side view of the VTe$_6$ octahedra forming the trigonal layers. (c) Side view of the high-temperature crystal structure of VTe$_2$. The conventional unit cell is indicated by the black solid lines. Vanadium atoms are in red, tellurium atoms are in teal.

TABLE I. Structural information for the high-temperature crystal structure obtained by using norm-conserving pseudopotentials.

Space group	164
Cell parameters	a=3.597 Å, b=3.597 Å, c=6.699 Å
Atomic positions (crystallographic coordinates)	V 1a
	Te 2d 0.255

II. LOW-TEMPERATURE CRYSTAL STRUCTURE OF VTe$_2$

A description of the low temperature crystal structure is given in the main text; for completeness here we report the conventional unit cell together with the structural information of this phase.
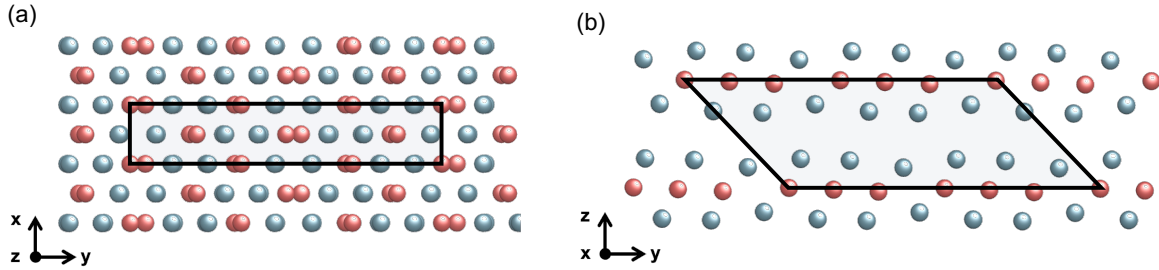

FIG. S2.   (a) Top view of the low-temperature crystal structure of VTe$_2$. (b) Side view of the low-temperature crystal structure of VTe$_2$. The conventional unit cell is indicated by the black solid lines. Vanadium atoms are in red, tellurium atoms are in teal.

TABLE II. Structural information for the low-temperature crystal structure obtained by using norm-conserving pseudopotentials.

Space group	12
Cell parameters	a=18.984 Å, b=3.595 Å, c=9.069 Å, β=133.3°
Atomic positions (crystallographic coordinates)	V 2a
	V 4i 0.361 0.0143
	Te 4i 0.707 0.795
	Te 4i 0.008 0.712
	Te 4i 0.356 0.728

III. PHONON CALCULATIONS OF THE HIGH-TEMPERATURE CRYSTAL STRUCTURE OF VTe$_2$

Fig. S3(a) shows the phonon dispersion along selected high symmetry directions of the first Brillouin zone for the normal phase of VTe$_2$ calculated using norm-conservative (top panel) and ultrasoft (bottom panel) pseudopotentials. For both pseudopotentials, none of the modes at Γ can be linked either to phonon A (characterized by a frequency of $\sim$1.65 THz, $\sim 55\,\mathrm{cm}^{-1}$ at 80 K) or to phonon B (characterized by a frequency of $\sim$2.50 THz, $\sim 85\,\mathrm{cm}^{-1}$ at 80 K). Indeed the lowest (non-zero) energy modes at Γ have a (nearly degenerate) frequency of $106\,\mathrm{cm}^{-1}$ (shown in Fig. S2(b) and (c)) and don't even involve the motion of the Vanadium atoms. Therefore the DFPT simulations performed on the high temperature phase of VTe$_2$ confirm the origin of the two phonon modes presented in the main text.

It is worth nothing that the phonon dispersions reported in Fig. S3 show the presence of negative phonon frequencies. Interestingly, the most negative frequency is found at q $= 2/3\,\Gamma$M, suggesting a large lattice instability towards the formation of a lattice reconstruction with triple periodicity along one in-plane direction [1], which is exactly what is observed in the CDW phase. Moreover, these large negative frequencies, in other CDW materials [1], have been connected to a predominant role played by the ions in the stabilization of the CDW phase.
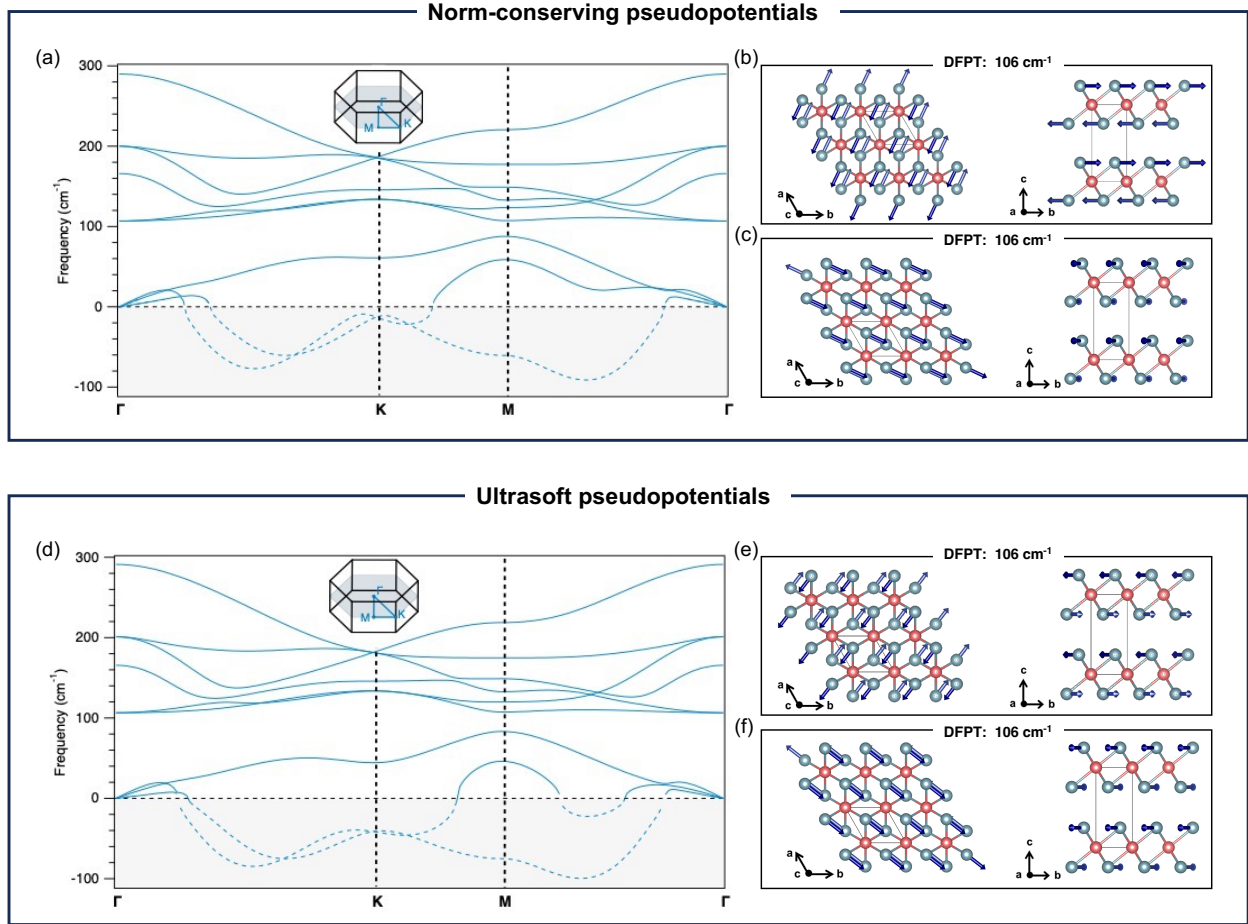
FIG. S3. (a) and (d) Phonon dispersion along selected high symmetry directions of the first Brillouin zone for the normal phase computed in the zero temperature limit. Results obtained with norm-conserving pseudopotentials (see Main Text) (optimized structural parameters: $a = 18.928$ Å, $b = 3.577$ Å, $c = 9.148$ Å and $\beta = 133.3°$) and with ultrasoft pseudopotentials (USPPs) from PS library [https://doi.org/10.1016/j.commatsci.2014.07.043] (optimized structural parameters: $a = 18.945$ Å, $b = 3.578$ Å, $c = 9.139$ Å and $\beta = 133.3°$). The most negative frequency at about $q = 2/3\,\Gamma M$ suggests the formation of a CDW phase with triple periodicity along one in-plane direction [1]. (b, c) and (e, f) Schematic representation of the two phonons with the lowest (non-zero) energy at the Γ point. For both phonon modes only the tellurium atoms are involved. Vanadium atoms are in red, tellurium atoms are in teal.

6

IV. ELECTRONIC DENSITY OF STATES OF VTe$_2$

Fig. S4 shows the projected density of states (PDOS) for the high-temperature phase (b) and CDW phase (c). For the CDW phase three different regions centered around -0.35, 0.70 and 1.45 eV can be identified in the PDOS. These regions are indicative of the bonding, nonbonding and antibonding bands arising from the trimerization-like displacements of the three adjacent vanadium atoms highlighted by the yellow oval in Fig. S4(a) and (d) [2–4]. This assignment is in agreement with the plots of Integrated Local Density Of States (ILDOS) acquired in an energy range of 0.01 Ry centered around -0.3 eV (bonding peak) and 0.70 eV (nonbonding peak) shown in Fig. S4(d) and (e).
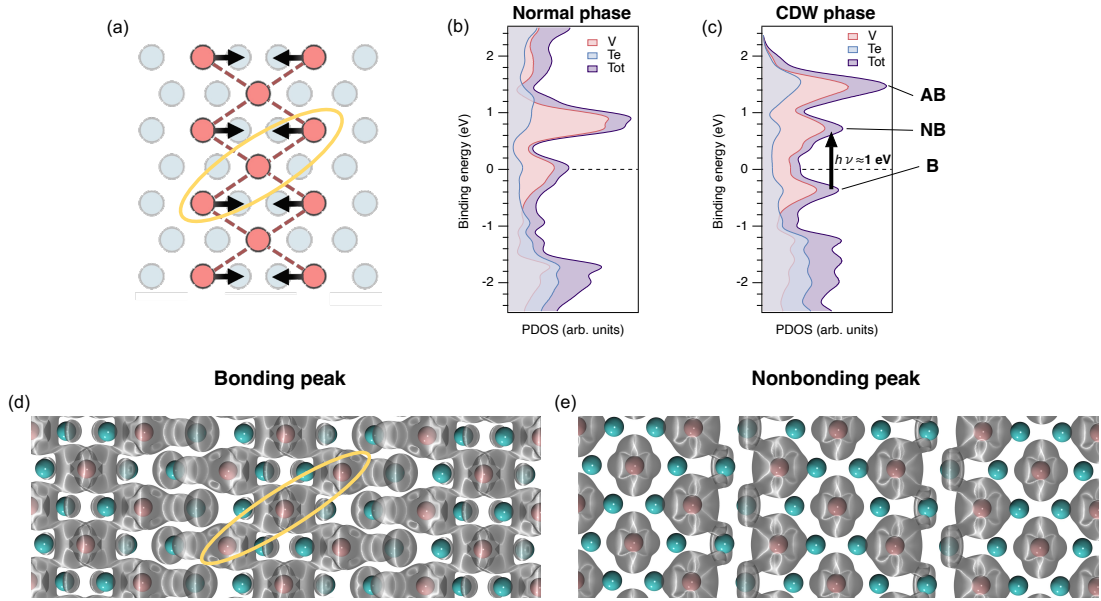

FIG. S4. (a) Top view of a VTe$_2$ layer in the low-temperature phase showing the lattice reconstruction that occurs in the CDW phase. The yellow oval shows the formation of the trimer-like bonding. (b, c) Calculated total density of states (DOS) and projected density of states (PDOS) for vanadium and tellurium atoms in the high temperature phase (b) and in the CDW phase (c). The black arrow in (c) shows the optical probe excitation resonant with the hybridized bonding and nonbonding vanadium states. (d,e) Integrated Local Density Of States (ILDOS) acquired in an energy range of 0.01 Ry centered around -0.3 eV (bonding peak) and 0.70 eV (nonbonding peak). The gray isosurface is characterized by an electron density of 0.1 e$^-$/a.u. Vanadium atoms are in red, tellurium atoms are in teal.

V. EVOLUTION OF THE PHASE OF THE PHONON MODES EXTRACTED FROM THE BROADBAND SUPERCONTINUUM MEASUREMENTS

Conventionally, the excitation of coherent phonons in opaque materials is described by the DECP theory [5]. Within this theory, the phase of the oscillation is directly related to the lifetime of the driving force on the vibrational coordinate. In the displacive limit, realized when the lifetime of the force is long compared to the period of the mode, a cosine oscillation is predicted ($\phi \approx 0, \pi$), while for the impulsive limit a sine oscillation is expected ($\phi \approx \pi/2$) [6, 7]. For VTe_2 a more complex situation emerges. Fig. S5 shows the evolution of the phase ($\phi_j(h\nu)$) of the two phonon modes as a function of the probe photon energy. While for the visible part of the spectrum the phase of both modes is constant and compatible with the displacive limit of the DECP model, in the infrared region of the spectrum we observe a continuous change in the phase of the modes extracted through our fitting procedure. We point out that the chirp correction of the broadband white light probe is performed with a curve common to all materials investigated with the same setup, leading to robust results. Hence we can exclude the trends shown in Fig. 5 are an artifact of the chirp correction; in particular the phase-slip between the two phonon modes in the near-infrared spectral range is evident from the data reported in Fig. 1c of the manuscript. Since the phase that characterizes the motion of the atoms is uniquely defined for each phonon mode, a photon-energy-dependent phase value must be a consequence of the probing mechanism. One possible explanation is connected to the peculiar way each phonon mode affects the band structure and the related optical properties. Since an optical transition that couples different bands spans a wide photon energy range, the distortion of these bands due to the excitation of a phonon mode (at a fixed time) entails a broadband reflectivity variation whose sign depends on the details of the dielectric function (see also [8]). In particular, this results in cosine oscillations of the reflectivity that can display an abrupt phase shift by a factor π across the central energy of an optical transition. This mechanism is discussed in [9]. In our case, we observe a smooth phase shift for both modes in the near-infrared spectral range, that cannot be accounted for by this simple qualitative model and suggests that in this spectral range multiple optical transitions affected by the phonon displacements overlap, leading to a phase of the oscillation that varies with the photon energy and is bound between 0 and π. This picture can be used to explain why in the infrared part of the

spectrum of in Fig. 1c of the main paper the oscillations due to the phonon appear to be slightly bent towards large pump-probe delays. Another explanation might be connected to the photon-energy-dependent probe depth. However, for both scenarios, in order to perform a quantitative analysis and to understand the microscopic origin of these phenomena, the knowledge of the equilibrium optical properties is required.
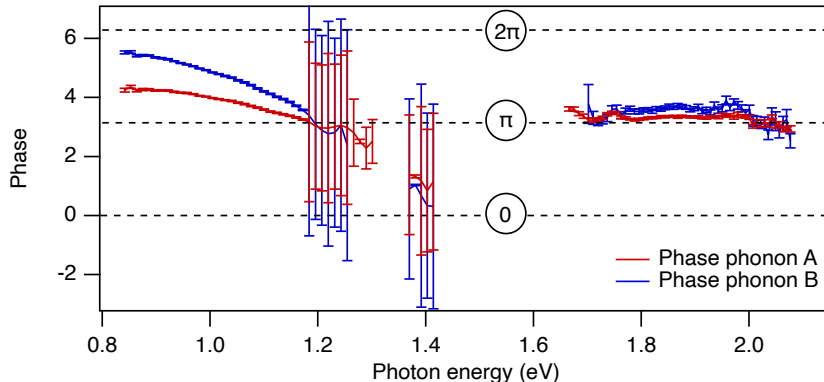

FIG. S5. Evolution of the phase ($\phi_j(h\nu)$) of the two phonon modes as a function of the probe photon energy. The value of the phase was extracted by fitting the data shown in Fig. 1(c) of the main paper using Eq. 1 presented in the main text. The regions of the spectrum with a poor signal-to-noise ration have been ignored, due to the difficulty to obtain reliable results. The large error bars for the values around $\sim1.2\,\mathrm{eV}$ and $\sim1.4\,\mathrm{eV}$ can be explained considering the fact that at these phonon energies the intensity of the two phonon modes is strongly reduced.

VI. TEMPERATURE EVOLUTION OF THE $\Delta R/R$ SIGNAL

With the aim of tracking the temperature dependence of both coherent and incoherent parts of the out of equilibrium reflectivity, we modeled the full temporal evolution after the perturbation (time zero, $t = 0$) as:

$$\frac{\Delta R}{R}(t,T) = G(t)\otimes$$
$$\left[\sum_{i=0}^{2} A_i(T)e^{-t/\tau_i^e(T)} + B(T) + \sum_{j=0}^{2} C_j(T)e^{-t/\tau_j^{ph}(T)}\cos(\omega_j(T)t + \phi_j(T)) \right], \quad (1)$$

where G(t) represents the cross correlation between the pump and probe pulses and corresponds to the temporal resolution of our experiments, which turns out to be $\approx 150\,\mathrm{fs}$.

$A_i(T)$ denotes the amplitude of the electronic relaxation phenomena with time constant $\tau_i^e(T)$. $B(T)$ represents the amplitude of much a slower process (likely related to the heating of the sample) that in our time window can be approximated by a constant term. Finally, $C_j(T)$ denote the amplitude of the oscillation due to the excitation of coherent phonons with angular frequency $\omega_j(T)$, phase $\phi_j(T)$ and decay time and $\tau_j^{ph}(T)$. Fig. S6(a) shows the evolution of the fit parameters presented in Eq. 1.
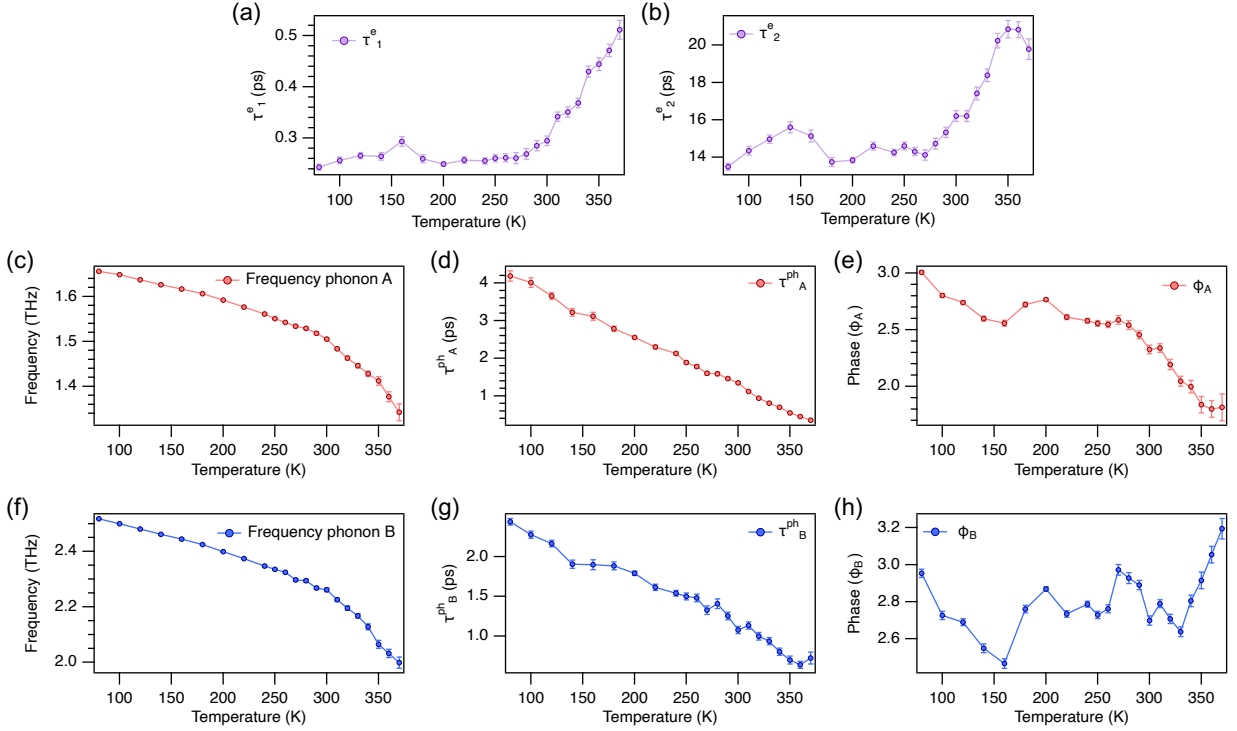

FIG. S6. Temperature evolution of the fit parameters of Eq. 1 with their error bars. (a) Time constant of the first (fast) electronic relaxation process. (b) Time constant of the second electronic relaxation process. (c-e) Frequency, decay time and phase of phonon A. (f-h) Frequency, decay time and phase of phonon B.

VII. SINGLE COLOR DOUBLE-PUMP TR-OS EXPERIMENTS

A. Modeling of the complete ΔR/R signal

With the aim of tracking the dependence of both coherent and incoherent parts of the out of equilibrium reflectivity on the delay between the two pump pulses (t_{pp}), we modeled the full temporal evolution after the perturbation (time zero, $t = 0$) as:

$$\frac{\Delta R}{R}(t, t_{pp}) = G(t) \otimes$$
$$\left[\sum_{i=0}^{2} A_{1,i}\, e^{-t/\tau_i^e} + B_1 + \sum_{j=0}^{2} C_{1,j}\, e^{-t/\tau_j^{ph}} \cos(\omega_j t + \phi_j) + \Theta(t - t_{pp}) \right.$$
$$\left. \left(\sum_{i=0}^{2} A_{2,i}\, e^{-(t-t_{pp})/\tau_i^e} + B_2 + \sum_{j=0}^{2} C_{2,j}\, e^{-(t-t_{pp})/\tau_j^{ph}} \cos(\omega_j (t - t_{pp}) + \phi_j) \right) \right], \quad (2)$$

where $G(t)$ represents the cross correlation between the pump and probe pulses while $\Theta(t)$ represents the Heaviside step function. $A_{p,i}$ denotes the amplitude of the electronic relaxation phenomena with time constant τ_i^e. B_p represents the amplitude of much slower process (likely related to the heating of the sample) that in our time window can be approximated by a constant term. Finally, $C_{p,j}$ denote the amplitude of the oscillation due to the excitation of coherent phonons with angular frequency ω_j, phase ϕ_j and decay time and τ_j^{ph}. The quantities with p=1 are used to describe the contribution arising from the first pump pulse while with p=2 are used to describe the contribution coming from the second pump pulse.

B. Extraction of the phase and amplitude evolution of the phonon modes

In order to extract the evolution of the amplitude and the phase of the two phonon modes we first removed the incoherent part of the signal by fitting the out of equilibrium reflectivity using the sum of four exponentially decaying functions (two decays are used to describe the relaxation process that take place after the arrival of each pump) and a constant background (used to take into account the amplitude of much slower process, likely related to the heating of the sample). After that, we modeled the temporal evolution of the coherent part of the signal after the perturbation induced by the arrival of the second pump pulse (t_{pp}) as:

$$\frac{\Delta R}{R}(t, t_{pp}) = I_A(t_{pp}) \, e^{-(t-t_{pp})/\tau_A^{ph}} \cos(\omega_A(t - t_{pp}) + \phi_A(t_{pp}))$$
$$+ I_B(t_{pp}) \, e^{-(t-t_{pp})/\tau_B^{ph}} \cos(\omega_B(t - t_{pp}) + \phi_B(t_{pp})), \tag{3}$$

where $I_i(t_{pp})$ denote the amplitude of the oscillation due to the excitation of coherent phonons with angular frequency ω_i, phase $\phi_i(t_{pp})$ and decay time and τ_i^{ph}.

C. Amplitude evolution of the phonon modes

The evolution of the amplitude of the two phonon modes has been described by using a model for independent oscillators [10, 11]. In particular, we modeled the temporal evolution of the intensity of the two modes after the perturbation induced by the arrival of the second pump pulse (t_{pp}) as:

$$I(t_{pp}) = I_i^0 e^{-(t-t_{pp})/\tau_i^{ph}} + \Delta I_i^0 \cos(\omega_i(t - t_{pp}) + \phi_i); \quad i = A, B \tag{4}$$

where I_i^0 is the amplitude of the phonon mode at the arrival of the second pump pulse and τ_i^{ph} is the decay time of the mode extracted from Eq. 3. ω_i and ϕ_i denote respectively the frequency and the phase of the phonon modes. Finally, the term ΔI_i^0 denotes the magnitude of the change in the intensity of the two phonon modes induced by the second pump pulse.

VIII. DOUBLE-PUMP BROADBAND TR-OS EXPERIMENTS

Fig. S7(a) shows the effect of a second excitation which is in phase with phonon B but almost completely out of phase with phonon A. The result is a strong enhancement in the amplitude of the former and a suppression of the latter in the complete energy range accessible through our supercontinuum probe. This first observation is confirmed by the square magnitude of FT reported in Fig. S7(b). Fig. S7(c) shows the opposite case. Indeed, the excitation of the second pump pulse here is in phase with phonon A but out of phase with phonon B. As shown by the FT transform reported in Fig. S7(d), after the arrival of the second pump pulse the amplitude of phonon B is almost completely suppressed in the entire spectral range.
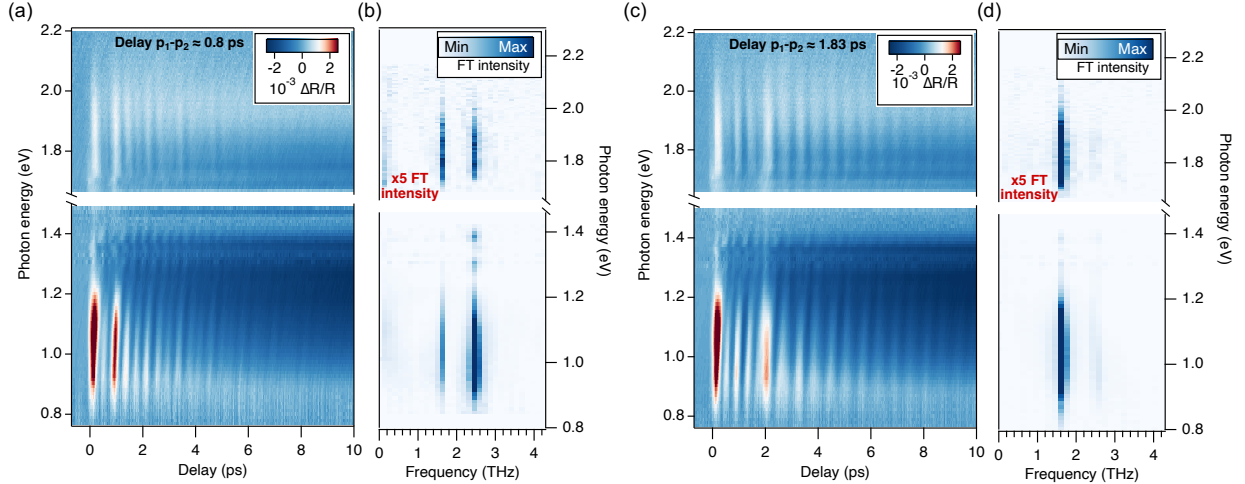
FIG. S7. Two dimensional maps showing the evolution of the $\Delta R/R$ signal of VTe_2, as a function of the probe photon energy (y-axis) and of the delay between the first pump and the probe pulses (x-axis). (a) Map acquired for a delay between the two pump pulses of $\sim$0.8 ps. (b) Two dimensional map showing the magnitude of the Fourier Transform (FT) of the coherent part of the $\Delta R/R$ signal extracted from (a) as a function frequency and of the probe photon energy. In the range between 1.6 and 2.2 eV the intensity of the FT has been multiplied by a factor 5. (c) Map acquired for a delay between the two pump pulses of $\sim$1.8 ps. The measurements have been performed at $\approx$ 80 K. (d) Two dimensional map showing the magnitude of the Fourier Transform (FT) of the coherent part of the $\Delta R/R$ signal extracted from (c) as a function of the frequency and of the probe photon energy. In the range between 1.6 and 2.2 eV, the intensity of the FT has been multiplied by a factor 5.

IX. SINGLE-PULSE INDUCED LATTICE HEATING

We estimated the single-pulse induced lattice heating of VTe_2 when illuminated by the pump pulse at an (incident) fluence of $\approx 490\,\mu J/cm^2$ to be of the order of $\approx 230\,K$. This estimate has been obtained by: i) computing the absorbed energy density ($\approx 110\,J/cm^3$), that requires the knowledge of the reflectivity ($R \approx 0.5$ at 800 nm) [12] and of the penetration depth ($\lambda \approx 22\,nm$ at 800 nm)[12]; ii) computing the volume of one formula unit and the number of atom it contains, and iii) considering the specific heat, that amounts to $\approx 45\,J/(mol\,K)$ [13]. The value obtained confirms that the lattice, heated by a single laser pulse, stays comfortably well below the CDW critical temperature in all the measurements

13

reported in the manuscript. Therefore, the fluence used in the experiments is enough to perturb the CDW gap, however it keeps the lattice below Tc.

---

[1] R. Bianco, L. Monacelli, M. Calandra, F. Mauri, and I. Errea, Weak dimensionality dependence and dominant role of ionic fluctuations in the charge-density-wave transition of NbSe$_2$, Phys. Rev. Lett. **125**, 106101 (2020).

[2] N. Mitsuishi, Y. Sugita, M. S. Bahramy, M. Kamitani, T. Sonobe, M. Sakano, T. Shimojima, H. Takahashi, H. Sakai, K. Horiba, H. Kumigashira, K. Taguchi, K. Miyamoto, T. Okuda, S. Ishiwata, Y. Motome, and K. Ishizaka, Switching of band inversion and topological surface states by charge density wave, Nature Communications **11**, 2466 (2020).

[3] N. Katayama, S. Tamura, T. Yamaguchi, K. Sugimoto, K. Iida, T. Matsukawa, A. Hoshikawa, T. Ishigaki, S. Kobayashi, Y. Ohta, and H. Sawa, Large entropy change derived from orbitally assisted three-centered two-electron σ bond formation in metallic Li$_{0.33}$VS$_2$, Phys. Rev. B **98**, 081104 (2018).

[4] M. H. Whangbo and E. Canadell, Analogies between the concepts of molecular chemistry and solid-state physics concerning structural instabilities. electronic origin of the structural modulations in layered transition metal dichalcogenides, Journal of the American Chemical Society **114**, 9587 (1992).

[5] H. J. Zeiger, J. Vidal, T. K. Cheng, E. P. Ippen, G. Dresselhaus, and M. S. Dresselhaus, Theory for displacive excitation of coherent phonons, Phys. Rev. B **45**, 768 (1992).

[6] D. M. Riffe and A. J. Sabbah, Coherent excitation of the optic phonon in si: Transiently stimulated raman scattering with a finite-lifetime electronic excitation, Phys. Rev. B **76**, 085207 (2007).

[7] E. M. Bothschafter, A. Paarmann, E. S. Zijlstra, N. Karpowicz, M. E. Garcia, R. Kienberger, and R. Ernstorfer, Ultrafast evolution of the excited-state potential energy surface of TiO$_2$ single crystals induced by carrier cooling, Phys. Rev. Lett. **110**, 067402 (2013).

[8] D. Soranzio, M. Peressi, R. J. Cava, F. Parmigiani, and F. Cilento, Ultrafast broadband optical spectroscopy for quantifying subpicometric coherent atomic displacements in WTe$_2$, Phys. Rev. Res. **1**, 032033 (2019).

[9] C. J. Sayers, S. Dal Conte, D. Wolverson, C. Gadermaier, G. Cerullo, E. Carpene, and E. Da Como, Spectrally resolving the phase and amplitude of coherent phonons in the charge density wave state of 1T-TaSe2, Advanced Optical Materials **10**, 2200362 (2022).

[10] L. Rettig, J.-H. Chu, I. R. Fisher, U. Bovensiepen, and M. Wolf, Coherent dynamics of the charge density wave gap in tritellurides, Faraday Discuss. **171**, 299 (2014).

[11] T. Onozaki, Y. Toda, S. Tanda, and R. Morita, Coherent double-pulse excitation of charge-density-wave oscillation, Japanese Journal of Applied Physics **46**, 870 (2007).

[12] H. Tanimura, N. L. Okamoto, T. Homma, Y. Sato, A. Ishii, H. Takamura, and T. Ichitsubo, Nonthermal melting of charge density wave order via nucleation in VTe_2, Phys. Rev. B **105**, 245402 (2022).

[13] A. A. Vinokurov, A. V. Tyurin, A. L. Emelina, K. S. Gavrichev, and V. P. Zlomanov, Thermodynamic properties of VTe_2, Inorganic Materials **45**, 480 (2009).